The micro-RWELL detector

M. Poli Lener[*]

Laboratori Nazionali di Frascati - INFN, Frascati, Italy
E-mail: marco.polilener@lnf.infn.it

G. Bencivenni, G. Felici, M. Gatta, G. Morello

Laboratori Nazionali di Frascati - INFN, Italy

R. De Oliveira

CERN, CH

A. Ochi

University of Kobe, Japan

The μ-RWELL is a compact spark-protected single amplification stage Micro-Pattern-Gaseous-Detector (MPGD). The detector amplification stage is realized with a polyimide structure, micro-patterned with a dense matrix of blind-holes, integrated into the readout structure. The anode is formed by a thin Diamond Like Carbon (DLC) resistive layer separated by an insulating glue layer from the readout strips. The introduction of the resistive layer strongly suppressing the transition from streamer to spark gives the possibility to achieve large gains ($> 10^4$), without significantly affecting the capability to be efficiently operated in high particle fluxes. In this work we present the results of a systematic study of the μ-RWELL performance as a function of the DLC resistivity. The tests have been performed either with collimated 5.9 keV X-rays or with pion and muon beams at the SPS Secondary Beamline H4 and H8 at CERN.

---

[*]Speaker.

1. Introduction

The μ-RWELL has been introduced as a thin, simple and robust detector for very large area applications requiring the operation in harsh radiation environment [1]. The detector, as sketched in fig. 1, is composed of two main components: the cathode and the μ-RWELL Printed Circuit Board (PCB), the core of the detector. The μ-RWELL-PCB, a multi-layer circuit produced with standard photo-lithography technology, is composed of three different elements: a suitably patterned Kapton® foil that acts as amplification stage of the detector; a grounded resistive layer as discharge limitation stage; a standard segmented copper electrode on a printed circuit board for readout purposes.

MPGDs, due to their typical micrometric distance of the electrodes, generally suffer from discharge occurrence that can eventually damage or destroy the detector as well as the associated front-end electronics or lead to dead time and detection inefficiencies. In the μ-RWELL, following the experiences with the MicroMegas [2] and the Micro Gap Resistive Plate Chambers (MGRPC) [3], this problem has been substantially solved with the introduction of a resistive layer on the bottom side of the Kapton® foil. The discharge suppression mechanism is the same of the resistive electrode used in the RPCs [4, 5, 6]: the streamer generated in the gas gap inside the amplification volume, inducing a large current through the resistive layer, generates a local drop of the amplifying voltage with an effective quenching of the multiplication process in the gas. This mechanism strongly suppressing the discharge amplitude (down to few tens of nano-ampere [1]) gives the possibility to achieve large gains with only one amplification stage.

A drawback, strictly correlated with the Ohmic behaviour of the detector is the reduced capability to be efficiently operated in high particle fluxes [1].

Finally the implementation of the resistive layer affects the charge spread on the readout electrodes (fig. 2): the charge collected on the resistive stage is dispersed with a time constant τ[7], dependent on the surface resistivity ρ_s and on the capacitive coupling with the readout.

Two different schemes have been studied for the resistive stage: the simplest layout, based on a homogeneous resistive layer, grounded at the edges (2D - current evacuation), in the following referred to as single-resistive layer, has been designed for low-rate applications; a more sophisticated one, based on a double-resistive layer with a proper density of through-vias between the two layers with the grounding done by means of the readout electrodes (3D - current evacuation) is under study for high-rate purposes. In this paper we focus on the single-resistive layout.

2. Detector architecture

The three prototypes used in this work are single-resistive layer detectors with DLC layer resistivity of 12/80/880 MΩ/□. One of the major difference of such detectors with respect to the first version of the μ-RWELL [1] is that the copper dots, patterned on the bottom side of the foil in correspondence of each WELL structure, have been removed thanks to the use of the DLC that ensures a high chemical and mechanical stability. Moreover a global irradiation test at the GIF++ CERN facility is in progress to study possible aging effects on the DLC. All prototypes under study were equipped with a readout patterned with a 400 μm pitch strips.
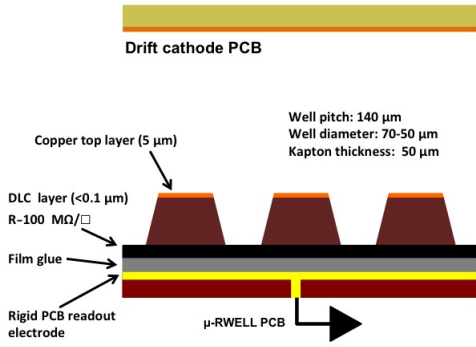
Figure 1: Sketch of the μ-Resistive WELL.
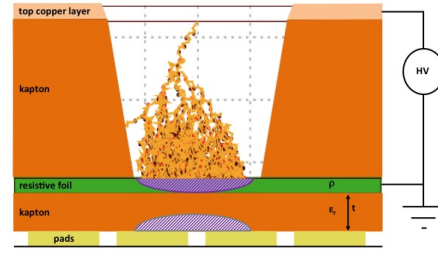
Figure 2: Sketch of the electronic avalanche in a μ-RWELL: the charge collected on the resistive layer induces the signal on the readout electrodes.

.

3. Detector characterization

The characterization of the detectors is performed with collimated 5.9 keV photons generated by an X-ray gun (PW2217/20 Philips). The gas gain of the detectors has been measured in current mode: the current drawn at a given potential through the resistive layer has been normalized to the ionization current, recorded operating the detector at unitary gain (very low voltage). The gain has been then plotted as a function of the amplification potential. As shown in fig. 3, the gas gain of the various detectors, measured for the Ar:i-C_4H_{10} (90:10) gas mixture, and parametrized as $G = e^{(\alpha \Delta V - \beta)}$, is typically ≥ 10000, being stopped when current instabilities (not discharges) are observed[1]: the largest gain is generally reached by the detector with highest resistivity. The rate capability has been measured at the gain G∼4000, well above the knee of the efficiency plateau (sec. 4). The X-ray gun can provide photon-converted signal rate ranging from 1 kHz up to approximately 300 kHz. The equivalent flux is obtained by dividing the measured rate by the irradiated area, given by the collimator surface[2] and for each flux we have plotted the ratio of the measured gain to the nominal gain at low rate (fig. 4). The points are fitted with the function

$$\frac{G}{G_0} = \frac{-1 + \sqrt{4 p_0 \Phi}}{2 p_0 \Phi} \tag{3.1}$$

introduced and derived in the appendix A of [1]. Reverting the eq. 3.1 we can obtain the value of the flux at a given normalized gain drop of 3%, representing our definition of the detector rate capability.

As expected, the gain decrease is correlated with the voltage drop due to current through the resistive layer: larger the DLC layer resistivity, the lower is the rate capability, ranging, for local irradiation, from few tens of kHz/cm^2 up to few MHz/cm^2, even though in case of global irradiation and large area detector we expect a rate capability much lower than the values measured with collimated X-rays.

---

[1]As shown in fig. 9 of [1]

[2]We performed a local irradiation of the detector with a 2.5 mm diameter brass collimator.
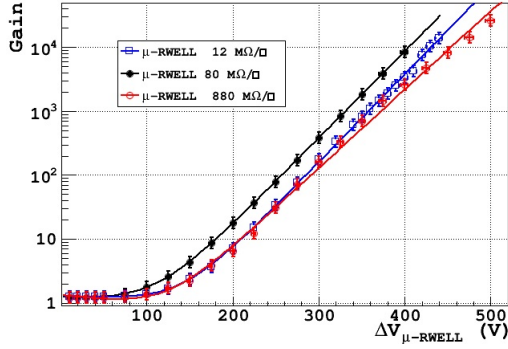
Figure 3: Measured gain for the three detectors.
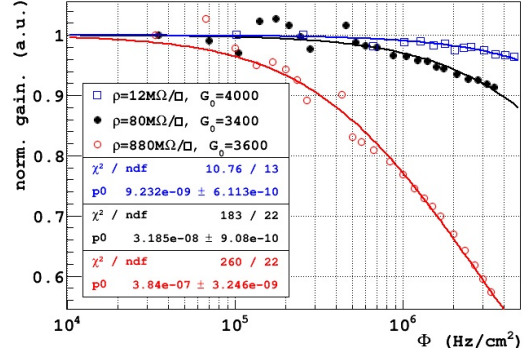
Figure 4: Normalized gain for 12 MΩ/□ (green triangles), 80 MΩ/□ (black full circles) and 880 MΩ/□ (red empty circles)

4. Beam test results

The tracking performance of the three detectors has been investigated at the H4-SPS CERN muon beam. The setup has been composed of four trigger scintillators (two read-out with Silicone Photomultipliers and two with Photomultiplier tubes) and two tracking stations each consisting of two triple-GEM detectors with two-dimensional strip readout. All gaseous detectors have been operated in $Ar{:}i{-}C_4H_{10}$ (90:10) at atmospheric pressure and were read-out with APV front-end cards [9], interfaced by the Scalable Readout System [10]. The APV chip, supplying analog output signals, allows the study of the detector tracking performance based on the charge centroid method. In fig. 5 the tracking efficiency of the detectors is reported as a function of the gain[3]: all detectors achieve a tracking efficiency above 98%. The shift of the efficiency curve of the 12 MΩ/□ prototype with respect to the others is correlated with the large charge spread occurring at low DLC resistivity (fig. 6): the charge dispersion on the readout strips increases, the signal collected by each pre-amplifier channel decreases thus requiring a higher gain to reach the full detector efficiency. The narrower residuals distribution, fig. 7, for the 80 MΩ/□ prototype has been obtained at a gain G$\sim$ 4000 with orthogonal tracks showing a standard deviation of 69 ± 1 μm. Subtracting the contribution of the external trackers ($\sigma_{fit} = 47 \pm 5$ μm), evaluated from the average width of their residuals[4], a spatial resolution of 52 ± 6 μm has been derived. Eventually, as reported in fig. 8, the space resolution depends on the resistivity of the DLC, showing a minimum around a surface resistivity of about 100-200 MΩ/□. At low surface resistivity the charge distribution loses the typical Gaussian shape and consequently the σ becomes larger.

At high surface resistivity the charge dispersion is so negligible (the strip cluster size being close to 1) that the charge centroid method becomes no more effective and the σ approaches the limit of pitch/$\sqrt{12}$.

---

[3]The tracking efficiency is defined as the ratio of the *good cluster of fired strips in the μ-RWELL* to the *total number of good tracks (reconstructed by the four external trackers)*; the good clusters are chosen to be inside $\pm 3\sigma$ of the residuals distribution.

[4]Defined as $x_{fit} - x_{meas}$, where x_{fit} is the intersection of the track, reconstructed with three detectors, with the excluded one and x_{meas} is its cluster centroid coordinate.
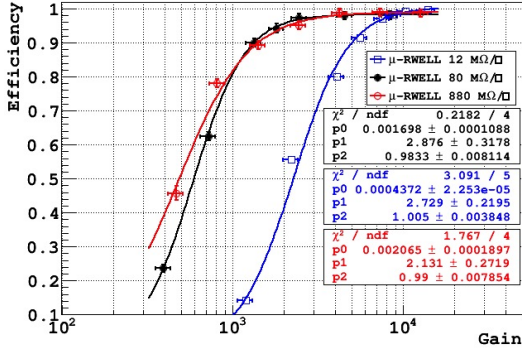
Figure 5: Tracking efficiency as a function of the gain for the three detectors.
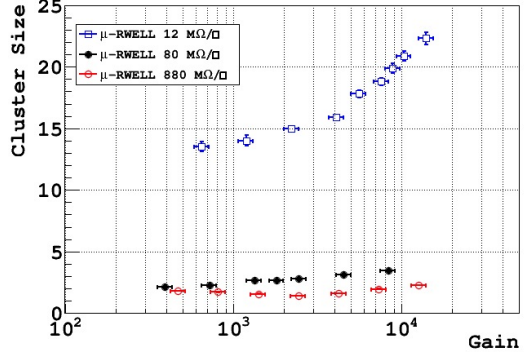
Figure 6: Strip cluster size (average number of contiguous fired strip per track) as a function of the gain for the three detectors.
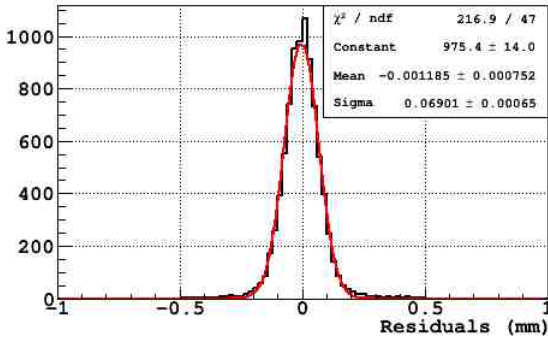
Figure 7: Residuals distribution for orthogonal tracks impinging the 80 MΩ/□ prototype.
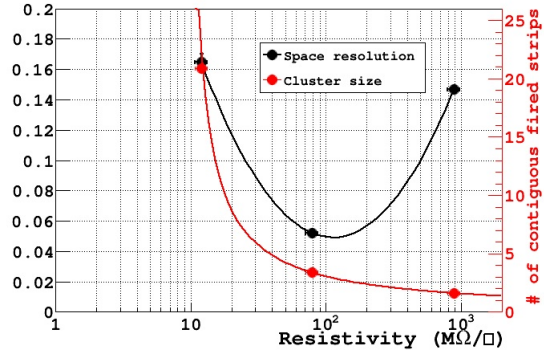
Figure 8: Residuals sigma and strip cluster size as a function of the DLC resistivity.

5. Large area μ-RWELL

In the framework of the CMS-phase2 muon upgrade the LNF-DDG group, in collaboration with the CMS groups present at LNF, INFN-Bologna and INFN-Bari, is developing a very large size μ-RWELL proposed for the installation in the CMS GE2/1 tracking wheels. A GE1/1-like μ-RWELL of ∼ 1.2×0.5 m^2 active area and segmented in 8 sectors has been built representing the largest micro-Resistive WELL ever built. Two sectors have been tested at the CERN SPS H8 test beam area, operating the detector with Ar:CO$_2$:CF$_4$ (45:15:40) and readout with VFAT2 Front-end electronics [11], in order to measure the time performance of the detector, with or-ed strips. The same test beam involved other two μ-RWELL Double Layer (DL) prototypes ($\rho_s \sim 40$ MΩ/□). The telescope has been composed of two GEM trackers, triggered by three scintillators.

The analysis is based on the selection of time coincidences of the events. Fig. 9 is an example reporting graphically the selections applied to TDC distributions relative to the external trackers and to the detector under examination. Such cuts reduce the μ-RWELLs TDC spectra to a gaussian-like

4
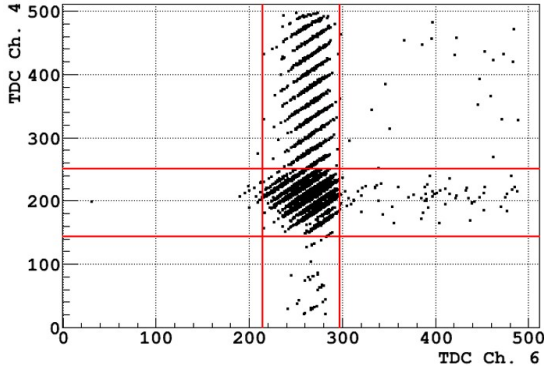
Figure 9: Distribution of the TDC events from the first external tracker correlated with the events collected by the large area μ-RWELL.
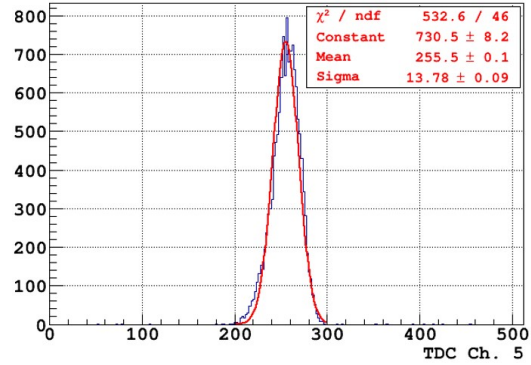
Figure 10: Example of TDC distribution for large μ-RWELL after TDC selection cuts.

distribution (fig. 10) that can be easily fitted. The σ_{TDC} must be deconvoluted by the contribution of the VFAT2 electronics in order to compute the time resolution of the detector, according to the formula [12]:

$$\sigma_t = \sqrt{\sigma_{TDC}^2 - \left(\frac{25\ \text{ns}}{\sqrt{12}}\right)^2} \tag{5.1}$$

The so-obtained σ_t have been measured as a function of the detector gain and they are shown in fig. 11. A clear saturation is visible at higher gain, when the σ_t approaches the value of 5.7 ns. It is natural to compare this value to the one measured with triple-GEM [13]: 4.5 ns equipping the detector with VTX chip and constant fraction discriminator (same gas mixture). The possibility to change the beam section dimensions has been exploited to integrate the rate capability points with lower fluxes, estimated using the counters and the MWPC present in the area which provide the beam profile in both dimensions. The detectors have been operated at different gain: $\sim 10^4$ for the DL prototypes, 6000 and 4000 for the two sectors of the large area and the relative variation of these values has been studied as a function of the different flux (fig. 12).

6. Conclusions

The μ-RWELL is a thin, simple and robust MPGD for very large area applications in harsh environment. The detector exhibits a gas gain up to and above 10^4 with Ar:i-C$_4$H$_{10}$ (90:10) gas mixture, a space resolution better than 60 μm and a tracking efficiency greater than 98% at a gas gain of 4000.
The rate capability for the single-resistive layout measured with a $\sim$3x3 cm^2 (FWHM) pion beam is larger than 35 kHz/cm^2, while for the double-resistive layout a rate capability better than 1 MHz/cm^2 has been achieved with X-rays. A time resolution down to 5.7 ns has been obtained for small as well as large area detector prototypes.
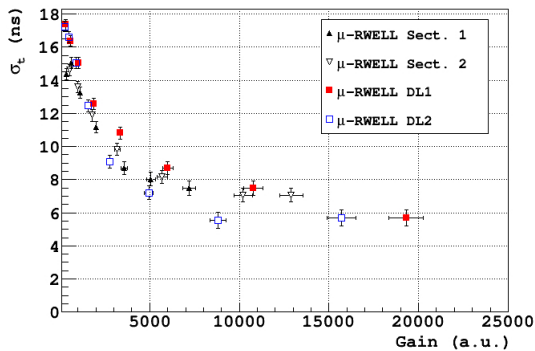
Figure 11: Time resolution as a function of the detector gain.
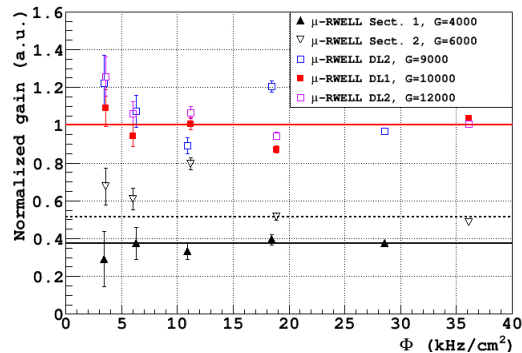
Figure 12: Gain variation as a function of the radiation fluence for the two sectors of the large area μ-RWELL (triangles) and for the small double layer prototypes (squares).

References

[1] G. Bencivenni at al., *The micro-Resistive WELL detector: a compact spark-protected single amplification-stage MPGD*, JINST 10 (2015) P02008.

[2] T. Alexopoulos et al., *A spark-resistant bulk-micromegas chamber for high-rate applications*, Nucl. Instr. & Meth. **A 640** (2011) 110-118.

[3] A. Di Mauro et al., *Development of innovative micropattern gaseous detectors woth resistive electrodes and first results of their applications*, arXiv:0706.0102.pdf

[4] Y. Pestov et al., *A spark counter with large area*, Nucl. Instr. & Meth. **93** (1971) 269.

[5] R. Santonico, R. Cardarelli, *Development of Resistive Plate Counters*, Nucl. Instr. & Meth. **A 377** (1981) 187.

[6] M. Anelli et al., *Glass electrode spark counters*, Nucl. Instr. & Meth. **A 300** (1991) 572.

[7] M.S. Dixit et al., *Simulating the charge dispersion phenomena in Micro Pattern Gas Detectors with a resistive anode*, Nucl. Instr. & Meth. **A 566** (2006) 281.

[8] A. Ochi et al., *Carbon sputtering Technology for MPDG detectors*, Proceeding of Science (TIPP2014) 351.

[9] M. Raymond et al., *The APV25 0.25 m CMOS readout chip for the CMS tracker*, IEEE Nucl. Sci. Symp. Conf. Rec. **2** (2000) 9/113.

[10] S. Martoiu et al., *Development of the scalable readout system for micro-pattern gas detectors and other applications*, JINST 8 (2013) C03015.

[11] P. Aspell et al., *VFAT2: A front-end system on chip providing fast trigger information, digitized data storage and formatting for the charge sensitive readout of multi-channel silicon and gas particle detectors*, URL:https://cds.cern.ch/record/1069906

[12] J. A. Merlin, *Etude de fonctionnement á long terme de détecteur gazeux l'environment á haut flux de CMS*, PhD Thesis (2016).

[13] G. Bencivenni et al., *Performance of a triple-GEM detector for high rate charged particle triggering*, Nucl. Instr. Meth. **A 494** (2002) 156.

6